Journal of Colloid and Interface Science 236, 242–251 (2001)
doi:10.1006/jcis.2000.7409, available online at http://www.idealibrary.com on IDEAL®

BNL-68062

Bivariate Extension of the Quadrature Method of Moments for Modeling Simultaneous Coagulation and Sintering of Particle Populations

Douglas L. Wright,* Robert McGraw,*,[1] and Daniel E. Rosner†

*Environmental Sciences Department, Atmospheric Sciences Division, Brookhaven National Laboratory, Upton, New York 11973-5000; and †Department of Chemical Engineering, Yale University, New Haven, Connecticut 06520-8286

Received April 10, 2000; accepted December 19, 2000

We extendthe application of moment methods to multivariate suspended particle population problems—those for which size alone is insufficient to specify the state of a particle in the population. Specifically, a bivariate extension of the quadrature method of moments (QMOM) (R. McGraw, *Aerosol Sci. Technol.* 27, 255 (1997)) is presented for efficiently modeling the dynamics of a population of inorganic nanoparticles undergoing simultaneous coagulation and particle sintering. Continuum regime calculations are presented for the Koch–Friedlander–Tandon–Rosner model, which includes coagulation by Brownian diffusion (evaluated for particle fractal dimensions, D_f, in the range 1.8–3) and simultaneous sintering of the resulting aggregates (P. Tandon and D. E. Rosner, *J. Colloid Interface Sci.* 213, 273 (1999)). For evaluation purposes, and to demonstrate the computational efficiency of the bivariate QMOM, benchmark calculations are carried out using a high-resolution discrete method to evolve the particle distribution function $n(v, a)$ for short to intermediate times (where v and a are particle volume and surface area, respectively). Time evolution of a selected set of 36 low-order mixed moments is obtained by integration of the full bivariate distribution and compared with the corresponding moments obtained directly using two different extensions of the QMOM. With the more extensive treatment, errors of less than 1% are obtained over substantial aerosol evolution, while requiring only a few minutes (rather than days) of CPU time. Longer time QMOM simulations lend support to the earlier finding of a self-preserving limit for the dimensionless joint (v, a) particle distribution function under simultaneous coagulation and sintering (Tandon and Rosner, 1999; D. E. Rosner and S. Yu, *AIChE J.*, 47 (2001)). We demonstrate that, even in the bivariate case, it is possible to use the QMOM to rapidly model the approach to asymptotic behavior, allowing an immediate assessment of when previously established asymptotic results can be applied to dynamical situations of current/future interest.

© 2001 Academic Press

Key Words: **moment methods; coagulation; sintering; aerosol dynamics; combustion aerosols.**

[1] To whom correspondence should be addressed.

The U.S. Government's right to retain a nonexclusive royalty-free license in and to the copyright covering this paper, for governmental purposes, is acknowledged.

1. INTRODUCTION

1.1. Background and Recent Developments

The method of moments (MOM) is a class of techniques for tracking preselected moments of a particle size distribution directly in space and time without explicit knowledge of the particle size distribution (PSD) itself (see, e.g., 1–3). Advantages include great computational efficiency, as only a few variables need to be integrated to accurately obtain important integral properties of the underlying PSD and freedom from numerical diffusion. Through recent developments summarized below, the MOM has become a powerful tool for representation of aerosol microphysical processes under rather general conditions. Important earlier limitations having to do with closure of the set of moment evolution equations have largely been overcome through the use of interpolation schemes for obtaining moments not explicitly tracked (4) or Gaussian quadrature–based moment schemes (5, 6) emphasized here. Indeed, the quadrature method of moments (QMOM) permits closure of the moment evolution equations for arbitrarily complex laws governing growth (5) and coagulation (6), and the method is free from the previously severe restrictions requiring an assumed PSD *shape*. Furthermore, although the distribution function itself remains unknown, integrals of known kernel functions over the distribution can still be accurately estimated using moment-based methods. In recent applications (5, 7–9), reliable estimates for aerosol physical and optical properties (generally within an accuracy of a few percent) were obtained using only the tracked lower order moments of the distribution. Perhaps the most extensive application of the method of moments to date has been to the representation of aerosol dynamics in regional-to-global scale atmospheric transport/transformation models (10). In this class of applications, which exploits the fact that the moments satisfy convective-diffusion equations of the standard form, simultaneous nucleation and aerosol dynamics are represented, and required physical and optical properties of the aerosol are estimated from the six lowest order radial moments of the local PSD.

0021-9797/01 $35.00
Copyright © 2001 by Academic Press
All rights of reproduction in any form reserved.

1.2. Moment Methods for Multivariate Population Balance Problems

This paper initiates the realistic extension of moment methods to multivariate population balance problems, defined here as those for which the particle distribution function depends on more than one internal coordinate (or particle 'state' variable). This can include the representation of generally mixed multicomponent aerosols, and/or evolving particles of complex morphology—indeed, the latter is the focus of the present study. We are motivated by the fact that, currently, the design and control of particle synthesis reactors is being impeded because, even for relatively simple flows, discrete, sectional, or finite difference numerical methods for solving the particle population balance equations (coupled with the host mixture flow) are too inefficient to be used for partially aggregated particle populations that require more than one or two state variables for their adequate description. Moreover, these methods may be "dead ends" when it comes to future incorporation into generally useful *turbulent* reactor codes currently needed by industry.

As a historical footnote, it is interesting that the pioneering application of moment methods to particulate systems by Hulburt and Katz (1) already considered, as an example, a bivariate form for evolution of the two radii of curvature of ellipsoidal particles in a continuously fed batch reactor. However, all subsequent MOM papers seem to be confined to the more tractable case of only a single radius, volume, or mass coordinate. Indeed, Hulburt and Katz did not actually complete a bivariate moment calculation, except to outline a possible solution for the overly restrictive special case that the growth law is independent of particle shape. More significantly, they certainly did not paint an optimistic prognosis for multivariate moment methods in general, citing such difficulties as the number of equations required to handle the larger number of ("mixed") moments, and analytic problems associated with reconstituting a bivariate distribution from bivariate moments. However, the intervening 35 years have seen unprecedented development in computational resources, along with the above-mentioned advances in the method of moments itself. In view of these developments, and the complexity of alternative simulation methods based on sectional discretization (see, e.g., 11–15), the feasibility of multivariate extensions of the MOM is ripe for reexamination.

1.3. Outline/Objectives of the Present Paper

In this paper we develop and illustrate a bivariate extension of the QMOM for modeling simultaneous coagulation and particle sintering. These processes occur in recently studied seeded laminar flames (16–18). The presently assumed condition of continuum regime Brownian coagulation, while not typical of nanoparticle synthesis in atmospheric pressure flames, was selected on account of the availability of comparable Monte Carlo numerical simulations for an established bivariate model (19), recently carried out by Tandon and Rosner (20) and Rosner and Yu (21). Calculations similar to those presented here that treat coagulation in the free-molecular regime are under way and will be reported separately. Details of the bivariate model, which uses particle volume (v) and surface area (a) as the state variables, are described in the cited papers. In Section 2 we call attention to the most important general features of the model, which includes simultaneous particle coagulation and finite-rate high-temperature sintering (coalescence) in a time-independent spatially uniform environment. Here we present a mathematical description of the simplest form of this bivariate model, including the dynamical equations for evolution of the associated mixed moments. Two implementations of bivariate QMOM model closure are presented in Section 3. It is important to note that these bivariate extensions of the QMOM require no further information about the distribution function other than its lower order mixed moments in order to evolve these moments to later times. This section also describes the high-resolution discrete model that will be used in Section 4 to evaluate the QMOM and to demonstrate its comparative efficiency. In Section 4 we compare our results for short to intermediate times with numerical benchmark calculations of the full bivariate distribution function obtained using this high-resolution discrete model. Time evolution of 36 preselected low-order mixed moments is obtained by numerical integration of the full distribution and compared with the corresponding moments obtained directly using the two above-mentioned bivariate implementations of the QMOM. With our more extensive implementation, errors of less than 1% are obtained. Moreover, longer time simulations using the QMOM (well beyond the reasonable computational range of the discrete model) are found to be in good agreement with the Monte Carlo–continuum regime results of Tandon and Rosner (20), lending support to their finding of a self-preserving asymptotic limit for the dimensionless joint particle distribution function, $n(v, a)$. Our results also display for the first time the approach to this asymptotic limit and thereby provide the time lag to effectively reach self-preserving behavior. We conclude in Section 5 with our recommendations for future work, which include comparing QMOM flame simulations to available experimental data (18). However, regarding the longer time horizon, we make the case that these techniques will probably also allow, in the foreseeable future, incorporation into full probability density function (PDF) methods for turbulent synthesis reactors of industrial interest, applying equally well to nanoparticle and microparticle synthesis covering the spectrum from the gas phase, to the liquid phase, and including (as an intermediate case of current industrial interest) supercritical fluids.

2. MATHEMATICAL MODEL

Taking particle volume and area as continuous variables, the particle distribution function $n(v, a)$ gives the number density of particles having volumes between v and $v + dv$ and surface areas between a and $a + da$. For the evolution of $n(v, a)$ due to

coagulation,

$$\left[\frac{\partial n(v,a)}{\partial t}\right]_{\text{coag}} = \frac{1}{2}\int_0^\infty \int_0^\infty \beta(v', v-v', a', a-a')n(v', a') \times n(v-v', a-a')\,dv'da' - n(v,a) \times \int_0^\infty \int_0^\infty \beta(v', v, a', a)n(v', a')\,dv'da'. \quad [1]$$

For simplicity and to illustrate our methodology, the coagulation rate, $\beta(u, v)$, between aggregates of sizes u and v is here considered to depend only on particle volume and not on aggregate surface area. For aggregates undergoing Brownian coagulation in the continuum regime this is taken to be

$$\beta(u, v) = K \cdot \left(u^{-1/D_f} + v^{-1/D_f}\right)\left(u^{1/D_f} + v^{1/D_f}\right), \quad [2]$$

where K is an environment-dependent proportionality constant and D_f is the particle fractal dimension (20). For Brownian coagulation of spherical particles $D_f = 3$.

For particles undergoing sintering, volume is conserved and evolution follows the continuity equation

$$\left[\frac{\partial n(v,a)}{\partial t}\right]_{\text{fusion}} = -\frac{\partial}{\partial a}[\dot{a}n(v,a)]. \quad [3]$$

We use the linearized expression of Koch and Friedlander (19) for the time rate of change of surface area for an individual aggregate,

$$\dot{a} = -\frac{1}{t_f}(a - a_{\min}), \quad [4]$$

where $a_{\min}$ is the area of the fully compacted (spherical) particle $[\pi(6v/\pi)^{2/3}]$ and t_f is the characteristic time of fusion/sintering.

We define the bivariate moments M_{kl} as

$$M_{kl} = \int_0^\infty \int_0^\infty v^k a^l n(v,a)\,dv\,da \quad [5]$$

and seek their evolution based on application of Eqs. [1]–[4]. following Tandon and Rosner (20) and Rosner and Yu (21), we assume that the particle surface area is, like the particle volume, additive during a coagulation event,

$$(v_1) + (v_2) \rightarrow (v_1 + v_2)$$
$$(a_1) + (a_2) \rightarrow (a_1 + a_2)$$

and thus the change in M_{kl} during the event involves the integrand multiplier

$$(v_1 + v_2)^k(a_1 + a_2)^l - v_1^k a_1^l - v_2^k a_2^l.$$

Multiplying this expression by the coagulation rate and integrating over the population distribution give the bivariate moment evolution equation

$$\left[\frac{dM_{kl}}{dt}\right]_{\text{coag}} = \frac{1}{2}\int_0^\infty \int_0^\infty \int_0^\infty \int_0^\infty [(v+v')^k(a+a')^l - v^k a^l - v'^k a'^l]\beta(v, v')n(v,a)n(v', a')\,dv'\,da'dv\,da. \quad [6]$$

Under sintering, the moments evolve according to

$$\left[\frac{dM_{kl}}{dt}\right]_{\text{fusion}} = \int_0^\infty \int_0^\infty v^k a^l \left[\frac{\partial n(v,a)}{\partial t}\right]_{\text{fusion}} dv\,da, \quad [7]$$

and using Eq. [3] and integrating by parts gives

$$\left[\frac{dM_{kl}}{dt}\right]_{\text{fusion}} = l\int_0^\infty \int_0^\infty v^k a^{l-1}\dot{a}n(v,a)\,dv\,da. \quad [8]$$

In keeping with the model of Tandon and Rosner (20), in addition to considering the collision frequency between aggregates a function only of particle volume and not of aggregate surface area, it is assumed that the characteristic fusion time t_f remains constant during the aggregation process, whereas in general t_f is a function of time through its dependence on the primary particle diameter (20). Both of these approximations have been made for simplicity to illustrate the method and it is apparent from the structure of Eqs. [6] and [8], which are already fully bivariate, that both approximations can be relaxed as modifications of this simplest form of the model become available in future applications of the bivariate QMOM.

3. MODEL SOLUTION

3.1. The Particle Size Distribution $n(v, a)$

While the primary focus of this paper is on moments, we begin this section with a description of the high-resolution discrete model that will be used for tracking the full particle size distribution in order to benchmark the accuracy of the moment methods. To solve for the particle size distribution $n(v, a)$ we use a bivariate generalization of the discrete scheme presented in McGraw and Wright (22). The two-dimensional version of the discrete approach introduced here uses a fixed logarithmic grid in both the area and volume coordinates, and because evolution processes create particle areas and volumes that do not correspond to any of the fixed points of the grid, these particles must be distributed over the fixed grid points. This is done as described below.

As an illustration, suppose there are N coagulation events between particles having the coordinates (v_i, a_i) and (v_j, a_j) grid points i and j) during an integration time step. This would yield N particles having the coordinates (v_k, a_k) with $v_k = v_i + v_j$ and $a_k = a_i + a_j$. In v–a space the point (v_k, a_k) falls within a quadrilateral of grid points. The material contained in the N particles is apportioned over the grid points of the quadrilateral such that the number of new particles N, the total

volume Nv_k, and the total surface area Na_k are each conserved during the apportionment.

During sintering, each of the n_i particles having surface area a_i has its area incremented by da_i ($da_i < 0$) during the time step, with $a_{i-1} < a_i + da_i < a_i$. The time step is kept small enough to ensure that the latter inequality is satisfied. The total surface area contained in the n_i particles of area $a_i + da_i$ is apportioned between enclosing grid points i and $i - 1$ such that for each of the n_i particles, surface area is conserved during apportionment. For simultaneous coagulation and sintering, operator splitting is used. The grid is extended far enough in each coordinate to ensure that the distribution amplitude is negligible at the high-volume, high-surface area end of the population spectrum.

Previous comparison of the one-dimensional version of this algorithm with the finite element method (FEM) results of Barrett and Webb (6) showed good agreement between the two approaches for the moments of $n(v)$ for coagulation. Exact solutions for the integral volume moments, available for constant-kernel coagulation, provide an important test of this approach, as it is the accuracy of the moments of the discrete scheme that is relevant for this work. Numerical results for the moments, obtained by integrating the discrete distributions, were found to be in excellent agreement with the corresponding exact moments. The handling of sintering is analogous to that of condensational growth—both of these are single particle processes and tend to suffer more from numerical diffusion than does coagulation, as is known from efforts to accurately model condensation using a fixed-bin sectional approach. Previous comparisons of results from this grid scheme for condensational growth with results from the method of characteristics (exact) show good agreement for $n(v)$ when sufficiently high grid resolution is used. There are both similarities and contrasts between our discrete model and the sectional models of Xiong and Pratsinis (14) and Seto *et al.* (23). Similarities include the use of a logarithmic grid in both the area and volume coordinates and in the use of flux conservation equations to consistently update the model at each time step. The main difference is that in the present approach the distribution is defined only at the grid points of the discrete model, whereas in the sectional approach a function of the size distribution, for example, the volume distribution function, is taken as constant within each section. We note that the recent work of Tsantilis and Pratsinis (15) implicitly allows for dynamical control of D_f in that aggregate shape is taken into account in computing the coagulation rate. Although the fractal dimension of each grid point could be computed from its coordinates (v_j, a_j), for simplicity the coagulation rate was evaluated using a constant D_f in all of our calculations using the discrete model.

3.2. *Quadrature Approaches to the Bivariate Moments M_{kl}*

The N-point quadrature expression for M_{kl} is

$$M_{kl} = \sum_{i=1}^{N} v_i^k a_i^l w_i, \qquad [9]$$

where each quadrature point $\{v_i, a_i, w_i\}$ has abscissas for both volume and area, as well as a weight. For the moment evolution equations we have the approximations

$$\left[\frac{dM_{kl}}{dt}\right]_{\text{coag}} \approx \frac{1}{2}\sum_{i=1}^{N}\sum_{j=1}^{N}\left[(v_i + v_j)^k (a_i + a_j)^l - v_i^k a_i^l - v_j^k a_j^l\right] \times \beta(v_i, v_j) w_i w_j \qquad [10]$$

and

$$\left[\frac{dM_{kl}}{dt}\right]_{\text{fusion}} \approx l \sum_{i=1}^{N} v_i^k a_i^{l-1} \dot{a}\,|_{a=a_i}\, w_i, \qquad [11]$$

where the approximate equalities refer to use of the quadrature approximation.

We present two quadrature techniques in this report: a multiple 3-point quadrature technique ($N = 3$) and a 12-point quadrature technique ($N = 12$). The latter is more computationally demanding but considerably more accurate. In each case we will propagate a square matrix $\mathbf{M}$ of 36 moments whose elements are the M_{kl} and both k and l take the values 0, 1/3, 2/3, 1, 4/3, and 5/3. Fractional rather than integral moments were chosen so that the k and l values remain small enough to not place too much emphasis on the tail of the distribution. It is useful to briefly discuss the rationale for selecting 36 moments. A description of the physical significance of the bivariate mixed moments for *selected* values of k and l has recently been presented (24). We do not attempt to attribute physical significance to each of the 36 mixed moments tracked in the present study, but view these instead as a basis set for approximation of quantities of interest that can be represented as weighted integrals over $n(v, a)$. Such quantities can include experimental observables and even other moments not included in the original set. Clearly, a finite set of mixed moments parameterizes the joint distribution $n(v, a)$ and constitutes an alternative description to the more obvious one of providing, say, an array of $n(v_i, a_i)$ values. Many moments of physical interest, including those for which the indices k and/or l are negative, can be adequately predicted using one of the 9-moment (3-point quadrature) descriptions furnished below (24). Use of 36 moments simply provides a larger basis enabling, as shown below, more accurate 12-point or multiple 3-point quadrature approximations than obtainable from a single 3-point quadrature derived from just 9 moments. Further consideration of the accuracy of quadrature approximations to weighted integrals over $n(v, a)$ based on 36 moments is given in Section 5. We now present a description of the multiple 3-point quadrature technique employed in the present calculations. While representative, the approach we describe here for multiple 3-point quadrature is not unique, and partitioning of the moments into different quadrature groupings may have certain advantages in other applications of the method (25).

The six diagonal elements of **M** are

$$M_{k,k} = \sum_{i=1}^{3} (v_i a_i)^k w_i \equiv \sum_{i=1}^{3} A_i^k w_i, \qquad [12]$$

where $A_i \equiv v_i a_i$. The superdiagonal and subdiagonal elements are

$$M_{k,k+1/3} = \sum_{i=1}^{N} a_i^{1/3} (v_i a_i)^k w_i \equiv \sum_{i=1}^{N} a_i^{1/3} A_i^k w_i \qquad [13a]$$

$$M_{k+1/3,k} = \sum_{i=1}^{3} v_i^{1/3} (v_i a_i)^k w_i \equiv \sum_{i=1}^{3} v_i^{1/3} A_i^k w_i, \qquad [13b]$$

respectively. Forming three ($k = 0,\ 1/3,\ 2/3$) symmetrized moments from these elements of **M**, we get

$$\frac{M_{k,k+1/3} + M_{k+1/3,k}}{2} = \sum_{i=1}^{3} \frac{(a_i^{1/3} + v_i^{1/3})}{2} A_i^k w_i. \qquad [14]$$

Equations [12] and [14] represent nine moments and these equations can be solved simultaneously to obtain three quadrature points $\{v_i, a_i, w_i\}$, $i = 1$–3. This is accomplished by first performing a one-dimensional quadrature with the diagonal moments using the routine ORTHOG of Press *et al.* (26), which will yield the $\{A_i, w_i\}$. Using these values of A_i and w_i in Eq. [14] converts Eq. [14] into a linear system of three equations in three unknowns which are solved for the sums $a_i^{1/3} + v_i^{1/3}$. Then for each $A_i = v_i a_i$ and sum $a_i^{1/3} + v_i^{1/3}$ one can solve a quadratic for the quadrature abscissas v_i and a_i.

The three quadrature points determined in this way can be used in Eqs. [10] and [11] to propagate any number of moments from their initial values. If the important pure volume ($l = 0$, first column of **M**) moments and pure area ($k = 0$, first row of **M**) moments were to be determined from quadrature points derived from the diagonal, subdiagonal, and superdiagonal elements of **M** only, one would not expect these three quadrature points to do an especially good job. To improve the accuracy of the estimated pure volume/area moments, one can perform additional 3-point quadratures to determine the $\{v_i, a_i, w_i\}$ optimal for the evolution of these moments. For example, whenever coagulation is done, the pure volume moments M_{k0} are used in a 3-point quadrature to obtain the set $\{v_i, w_i\}$, $i = 1$–3. Then using these $\{v_i, w_i\}$ in Eq. [9] for $M_{k,1/3}$ for $k = 1,\ 4/3,\ 5/3$ one again gets a linear system of three equations in three unknowns which can be solved for the three a_i yielding the full set $\{v_i, a_i, w_i\}$. Whenever sintering is done, an analogous procedure is performed using the pure area moments M_{0l} together with the moments $M_{1/3,l}$ for $l = 1, 4/3, 5/3$.

The 12-point quadrature technique employs all 36 elements of **M** to obtain 12 quadrature points $\{v_i, a_i, w_i\}$ such that each of the 36 moments is exactly given by Eq. [9] with these points. That is,

$$M_{kl} = \sum_{i=1}^{12} v_i^k a_i^l w_i. \qquad [15]$$

These 12 quadrature points are determined with the aid of the conjugate-gradient minimization algorithm outlined in (26). From an initial guess of the quadrature parameters $\{v_i, a_i, w_i\}$, $i = 1$–12, a 36-dimensional minimization is used to locate values of the parameters that satisfy Eq. [15]. This search is driven by minimization of the squared differences between the actual moments and moments computed via Eq. [15] by minimization of the function

$$F(\mathbf{v}, \mathbf{a}, \mathbf{w}) = \sum_{i=0}^{5} \sum_{j=0}^{5} \left[\frac{M_{i/3,j/3}(\mathbf{v}, \mathbf{a}, \mathbf{w}) - M_{i/3,j/3}}{M_{i/3,j/3}} \right]^2, \qquad [16]$$

where $\mathbf{v} = \{v_i\}$ and likewise for **a** and **w**. Constraints are imposed to ensure that the w_i remain positive by modification of the expressions for $\partial F(\mathbf{v}, \mathbf{a}, \mathbf{w})/\partial w_i$.

A 36-dimensional minimization would be expected to be difficult and very demanding computationally, but two circumstances facilitate the computation. First, an excellent initial guess for the set $\{v_i, a_i, w_i\}$ can be obtained from the quadrature parameters obtained from the multiple 3-point technique described above, supplemented by one additional quadrature (similar to the second and third quadratures above) using the last row (or column) of **M** in conjunction with three other appropriate M_{kl}. The quadrature parameters from four 3-point quadratures can be grouped into a single set of 12 yielding a set $\{v_i, a_i, w_i\}$, $i = 1$–12, and with the w_i renormalized by a factor of 4, this set of 12 parameters used in Eq. [15] yields all 36 M_{kl} to within a few percent. Thus this set provides an excellent initial guess for the minimization routine.

The second and more important circumstance is that as the integration of the moment evolution equations proceeds, the values of $\{v_i, a_i, w_i\}$ consistent with the M_{kl} at time $t + dt$ differ ever so slightly from the known values consistent with the M_{kl} at time t. Thus relatively few iterations of the minimization algorithm are required to nudge the quadrature parameters along so that they remain consistent with the moments as they evolve. At each time step, increments to the moments are computed from Eqs. [10] and [11] from the current set $\{v_i, a_i, w_i\}$ (which are consistent with the current moments) and the moments are updated. The updated moments are then used in Eq. [16] to advance the $\{v_i, a_i, w_i\}$ until they yield the updated moments to within about 0.001%. We have found this approach to be surprisingly efficient; only about 10 min CPU time was required on a PC (Pentium II processor) for the calculation shown in Fig. 2 using the 12-point quadrature technique, although we note that efficient coding of Eq. [16] and its partial derivatives is essential to this performance. Though less accurate, the multiple 3-point quadrature technique is about 100 times faster than the 12-point technique.

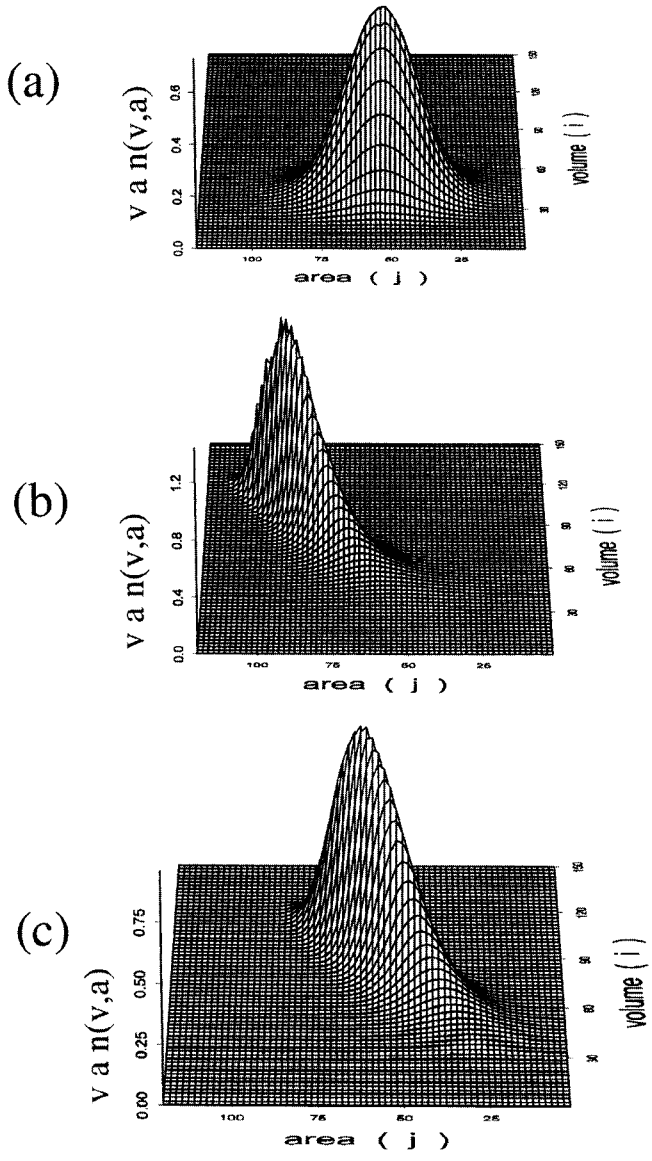

FIG. 1. Joint volume–surface area distribution $v\,a\,n(v,a)$ used as a test case, with $n(v,a)$ normalized to unity, at (a) $\tau = 0$, (b) $\tau = 10$ for evolution under coagulation alone, and (c) result at $\tau = 10$ for evolution under simultaneous coagulation and sintering. The time coordinate is $\tau = KM_{00}(0)t$, where K is the constant appearing in the coagulation kernel, Eq. [2]. The horizontal scales are logarithmic in particle volume and surface area and indicate the grid point number for each coordinate; volume$(i) \equiv v_i = v_{\min} S_v^{i-1}$ and area$(j) \equiv a_j = a_{\min}(v_i) S_a^{j-1}$, where S_v and S_a are constant scale factors, $v_{\min}$ is the volume of the smallest grid point, and $a_{\min}(v_i)$ is the minimum surface area for a particle of volume v_i. For each v_i, the first grid point in the area coordinate is the minimum area for that particle volume (corresponding to a spherical particle), and the largest value of a for that v_i is $100 a_{\min}(v_i)$. Thus the extent to which the distribution projects in the area coordinate is a measure of the degree to which the particles are noncompact and thus have fractal dimensions (D_f) less than 3. $S_v = 1.06825$, $S_a = 1.03118$, and $v_{\min} = 0.05341$.

4. RESULTS

The initial test distribution was taken as lognormal in both coordinates (Fig. 1a). For the cases of coagulation alone and simultaneous coagulation and sintering, the grid contained 150 points in each coordinate and each of these benchmark calculations using the bivariate discrete scheme of Section 3.1 required about 10 calendar days on a Sun Spark Enterprise computer. The coagulation kernel was evaluated setting $D_f = 3$ in Eq. [2]. For the case of sintering alone, a larger grid of 1000 points in each coordinate could be run in tolerable computation time. The time coordinate is $\tau = KM_{00}(0)t$, where K is the constant appearing in the coagulation kernel of Eq. [2] and $M_{00}(0)$ is the initial particle number density. Figure 1 shows the normalized initial [$\tau = 0$; $M_{00}(0) = 1$] distribution (Fig. 1a) and the final ($\tau = 10$) distributions for both the cases of coagulation alone (Fig. 1b) and the simultaneous coagulation and sintering (Fig. 1c). The conditions are $K = 1$ and $t_f = 10$ in Eqs. [2] and [4], respectively. Note that the area and volume scales are logarithmic and that the distribution undergoes substantial evolution in both of these cases. Thus the average particle volume ($\bar{v} = M_{10}/M_{00}$) and average surface area ($\bar{a} = M_{01}/M_{00}$) change from the initial values $\bar{v}(0) = 1.0$ and $\bar{a}(0) = 25.8$ to $\bar{v}(10) = 22.25$ and $\bar{a}(10) = 574.5$ under coagulation alone and to $\bar{v}(10) = 22.25$ and $\bar{a}(10) = 240.3$ under simultaneous coagulation and sintering.

Figure 2 shows the time evolution for 18 of the 36 bivariate moments modeled in this study, as computed from both the

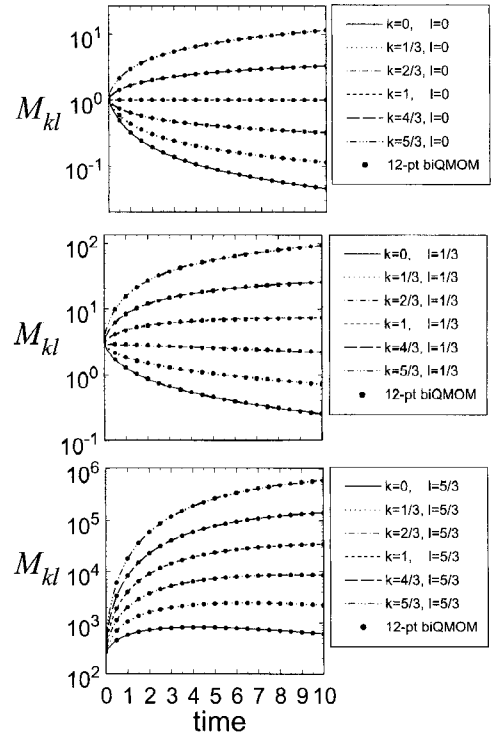

FIG. 2. Comparison of the time evolution for 18 of the 36 bivariate moments obtained from the 12-point bivariate extension of the QMOM and from the 150×150 discrete representation of the full bivariate distribution function, for simultaneous coagulation and sintering. The time coordinate is $\tau = KM_{00}(0)t$, where K is the constant appearing in the coagulation kernel, Eq. [2]. The various curves may be distinguished by noting that the k-index increases from the lowest to the highest curves shown in each panel of the figure.

150 × 150 discrete model and the 12-point bivariate extension of the QMOM. These results are for simultaneous coagulation and sintering and are for the same conditions and time period as in Fig. 1 ($\tau = 0$–10). The 12-point quadrature approach yields excellent tracking of all moments, with errors [(quadrature–exact)/exact 100%] not exceeding 1% over the full set of 36 moments, including those not shown in the figure. (The term "exact" refers here to the moments obtained by numerically integrating the full PSD from the high-resolution discrete model as a function of time.) For the separate processes of coagulation and sintering, the errors also did not exceed 1%. For the multiple 3-point quadrature technique, all three cases studied (coagulation, sintering, and simultaneous coagulation and sintering) gave errors in the range 0–7% with the largest errors encountered for the highest order moments.

Figure 3 shows evolution for 18 of the computed 36 dimensionless bivariate moments

$$\mu_{kl} = \left(\frac{M_{kl}}{M_{00}}\right)\left(\frac{M_{00}}{M_{10}}\right)^k\left(\frac{M_{00}}{M_{01}}\right)^l \qquad [17a]$$

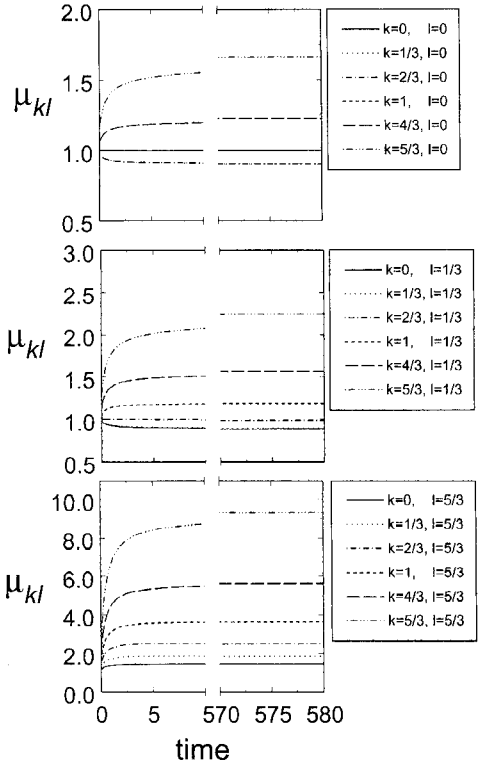

FIG. 3. Time evolution for 18 of the 36 dimensionless bivariate moments toward their asymptotic values (see also Table 1) for simultaneous coagulation and sintering for fractal dimension $D_f = 2.5$ and nondimensional time constant ratio $\mathrm{Dam_f} = [KM_{00}(0)]^{-1}/t_f = 10^{-4}$. The time coordinate is $\tau = KM_{00}(0)t$, where K is the constant appearing in the coagulation kernel, Eq. [2]. The split scale shows both the initial time evolution ($\tau = 0$–10), highlighting the approach to asymptotic behavior, and the evolution at considerably longer times ($\tau = 570$–580), in which the reduced moments have assumed essentially constant values characteristic of the asymptotic regime. These results were obtained using a single 3-point quadrature as described in the text.

TABLE 1
Asymptotic Values of the Dimensionless Bivariate Moments for $D_f = 2.5$, $\mathrm{Dam_f} = 10^{-4}$

	$k = 0$	$k = 1/3$	$k = 2/3$	$k = 1$	$k = 4/3$	$k = 5/3$
$l = 0$	1.000000	0.906171	0.904653	1.000000	1.225794	1.661185
$l = 1/3$	0.882725	0.893132	0.984853	1.185555	1.560478	2.240350
$l = 2/3$	0.895444	0.985409	1.166676	1.493252	2.072759	3.111479
$l = 1$	1.000000	1.166718	1.454857	1.953273	2.832171	4.412098
$l = 4/3$	1.183588	1.441677	1.875104	2.624132	3.953228	6.358280
$l = 5/3$	1.450848	1.832549	2.476687	3.601437	5.615130	9.284314

and their approach to the self-preserving limit. The moments, M_{kl}, and reduced moments, μ_{kl}, are functions of time, but this dependence has been suppressed in Eq. [17a] to simplify notation. Note that these are the same dimensionless moments of the joint PDF (ψ_{12}) studied by Tandon and Rosner (20) in the asymptotic limit ($t \to \infty$) using the Monte Carlo method:

$$\mu_{kl}(t) = \int_0^\infty \int_0^\infty \eta_1^k \eta_2^l \cdot \psi_{12}(\eta_1, \eta_2, t) \cdot d\eta_1 d\eta_2. \qquad [17b]$$

In Eq. [17b], η_1 is particle volume divided by the average particle volume ($\eta_1 = v/\bar{v}$) and η_2 is particle surface area divided by the average particle surface area ($\eta_2 = a/\bar{a}$). The results shown in Fig. 3 were obtained under simultaneous coagulation and sintering using a single 3-point quadrature derived from the six diagonal elements of **M**, together with the three additional symmetrized moments of Eq. [14], by solving Eqs. [12] and [14]. The evolution shown in Fig. 3 is carried out for considerably longer times than the results of Figs. 1 and 2 (well beyond the tolerable computational time range of the high-resolution discrete model) in order to show the approach of these reduced moments to asymptotic values characteristic of a self-preserving limit for the bivariate distribution. Asymptotic values for the full set of computed dimensionless bivariate moments are provided in Table 1. The lag times required to reach the asymptotic limit are evident in the short-time behavior shown in Fig. 3. Note that in the top panel of Fig. 3 only four curves are clearly distinct. This is due to the near coincidence in curves corresponding to the pairs $k = 0, 1$ and $k = 1/3, 2/3$ (see also Table 1). Similarly in the second panel the results for $k = 0$ and $k = 1/3$ are nearly coincident. When the pure volume moments M_{k0} are treated on a self-evolving basis (results not shown), the evolution of these moments reduces to that of the univariate case, and very accurate results for these moments are obtained. Application of the univariate QMOM to pure coagulation, with extension to the self-preserving limit, will be reported in future work (22). Note that the similarity variable for coagulation alone is the expected nondimensional volume ratio $v/\bar{v}$ as follows from Eq. [17] for $l = 0$. For simultaneous coagulation and sintering, we define the nondimensional Damkohler number $\mathrm{Dam_f} = [KM_{00}(0)]^{-1}/t_f$. The asymptotic values of the mixed moments shown in Fig. 3 are in reasonably good agreement

with the values calculated independently from Monte Carlo simulation of the full asymptotic distribution for these conditions: $D_f = 2.5$ and $\mathrm{Dam}_f = 10^{-4}$ (see Fig. 4 for comparison). Note that sintering plays a considerably less important dynamical role than does coagulation at $\mathrm{Dam}_f = 10^{-4}$.

Figure 4 presents a comparison between the bivariate QMOM simulation results in the asymptotic limit and the results of Monte Carlo (MC) simulations reported by Tandon and Rosner (20). The QMOM asymptotic moments are obtained as in Fig. 3 and the values of D_f and Dam_f are varied to match the conditions of the MC simulations. The particle size distributions from the MC simulations are reduced distributions in the asymptotic limit with moments that should be compared with the corresponding reduced moments from Eq. [17] also in the asymptotic limit. The MC moments used for this comparison are derived from the values reported by Tandon and Rosner (20) upon making a rescaling transformation as now described: From Eq. [17a] it is evident that

$$\mu_{00} = \mu_{01} = \mu_{10} = 1 \qquad [18]$$

for the reduced moments. Slight departures from these normalization conditions were encountered in the MC calculations, most likely resulting from limitations of statistical sampling, and these departures result in amplified error in the higher order moments. Accordingly, we found it necessary to rescale the previously reported MC moments, in order to satisfy Eqs. [18]. The following two-step process was used: First, the previously reported moments were normalized by μ_{00}^{MC} such that the renormalized moment $\tilde{\mu}_{00}^{\mathrm{MC}}$ is now unity. In the second step let $\tilde{\mu}_{10}^{\mathrm{MC}} = 1 = v_{\mathrm{scale}}\mu_{10}^{\mathrm{MC}}$ and $\tilde{\mu}_{01}^{\mathrm{MC}} = 1 = a_{\mathrm{scale}}\mu_{01}^{\mathrm{MC}}$, where μ^{MC} and $\tilde{\mu}^{\mathrm{MC}}$ denote the original (20) MC moments—after renormalization by μ_{00}^{MC}—and the rescaled MC moments, respectively. The preceding relations determine the two scaling parameters v_{scale} and a_{scale}, which we then used to scale the remaining moments according to $\tilde{\mu}_{kl}^{\mathrm{MC}} = (v_{\mathrm{scale}})^k\,(a_{\mathrm{scale}})^l\,\mu_{kl}^{\mathrm{MC}}$. This forces the scaled moments corresponding to those in Eq. [18] to be unity and solves other problems with the original MC moment sets. For example, because μ_{00} and $\mu_{1,0}$ are exactly unity, intermediate moments such as $\mu_{1/2,0}$ must be less than unity—this is because of the convexity criterion that must be satisfied by any valid set of moments of a distribution of a random variable (27). Specifically, $\mathrm{Log}(\mu_{k0})$ must be a convex function of k. The original MC moments miss this dip below unity, probably due to their overestimation of μ_{10}. The same argument holds for the pure area moments ($k = 0$) leading to the requirement that $\mu_{0,1/2}$ be less than unity.

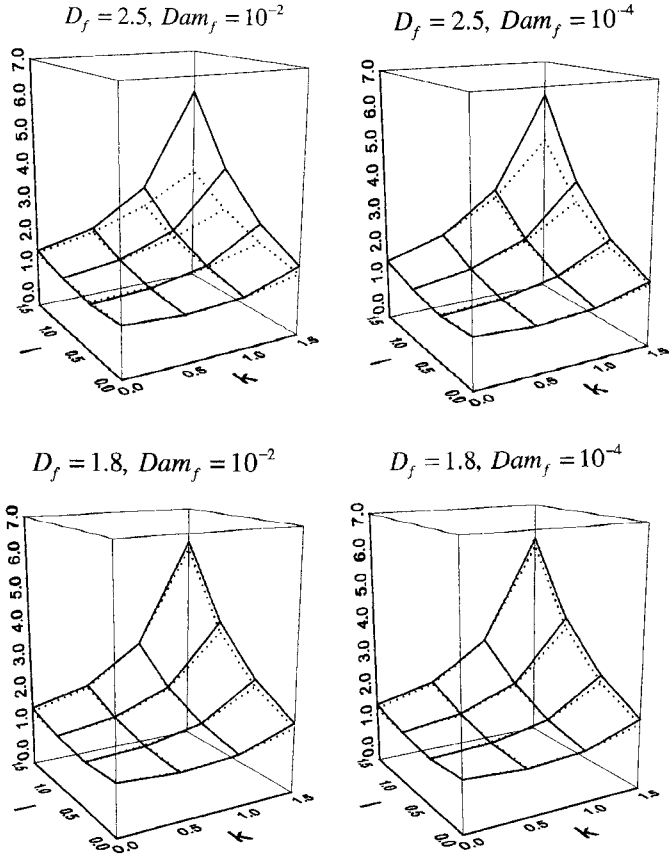

FIG. 4. Comparison of asymptotic reduced moments from Monte Carlo (dotted line grid) and 3-point QMOM simulation (solid line grid). The Monte Carlo moments have been rescaled to satisfy Eq. [18] following the procedure described in the text.

Figure 4 shows the rescaled moments $\tilde{\mu}^{\mathrm{MC}}$ at the half-integer values of k and l reported by Tandon and Rosner (20) (indicated by the intersection points on the dotted grid) together with the corresponding values obtained using a single 3-point quadrature as described in connection with Fig. 3 (indicated by the intersection points on the solid line grid). Half-integer moments for the QMOM were obtained from the neighboring $\frac{1}{3}$-fractional moments by 3-point Lagrangian interpolation of $\mathrm{Log}(\mu_{kl})$. This interpolation scheme is similar to the method used by Frenklach and Harris (4) to estimate fractional moments and has the property that it is exact for lognormal distributions. The agreement shown in Fig. 4 lends support to the finding of Tandon and Rosner (20) that for the case of continuum regime Brownian coagulation, the notion of self-preserving asymptotic shape extends to the bivariate populations using $v/\bar{v}$ and $a/\bar{a}$ as similarity variables (cf. Eq. [17]). Specifically, the asymptotic values of the mixed moments obtained from the bivariate QMOM are seen to be in good agreement with the values calculated independently from Monte Carlo simulation of the full asymptotic distributions (20). This agreement also validates the new approach for long-time simulation, demonstrating that the quadrature method of moments can provide reliable characterization of the asymptotic limit as well as of the dynamics. The fact that this agreement was obtained using only a single 3-point quadrature (9 moments) suggests that fewer than 36 moments can be used, if required, and reasonably accurate results in a fully bivariate calculation can still be obtained.

Finally, it is interesting to note that the dimensionless moments show only a very weak sensitivity to changes in D_f.

Indeed, taking the formal limit $D_f \to \infty$ in Eq. [2] yields a constant coagulation kernel case with analytic results for the dimensionless moments that are not significantly different from numerical results for continuum Brownian coagulation with $D_f = 3$. The insensitivity to D_f may be explained by noting that the continuum Brownian kernel is itself nearly constant, except when the coagulating particles are of very different sizes. More precisely, for $1/140 \leq u/v \leq 140$, the Brownian kernel differs from a constant value by at most 30% (28). Thus the asymptotic values of the pure volume moments ($l = 0$) shown in Table 1 for $D_f = 2.5$ are quite close to the asymptotic reduced moments obtained by Vemury *et al.* (29) for $D_f = 3$. Physically, the insensitivity to D_f in the continuum regime results because the effect of enhanced collision area, with reduction of fractal dimension below $D_f = 3$, is reduced by the increased drag of the agglomerates (30).

5. OUTLOOK AND SUMMARY

Extension of quadrature-based moment methods to potentially important trivariate distribution functions (e.g., those requiring an additional state variable for chemical composition) is probably now within reach of the kind of quadrature approach developed here, with important implications for the process modeling of turbulent nanoparticle synthesis reactors, including turbulent "sooting" combustors. Indeed, work along these lines has been initiated, and will be reported in future publications. Whether this approach is possible for describing populations requiring more than three state variables, or whether rather different (or perhaps 'hybrid') methodologies will be required, remains to be seen. A major application for multivariate moment methods, with multiple state variables, would be to modeling the dynamics of generally mixed, multicomponent particle populations as well as to particle populations having both mixed composition and complex shape. Generally mixed multicomponent particle populations are described by a fully multivariate distribution function $f(m_1, m_2, \ldots)$, where m_i is the mass of component i in the particle. Currently, most aerosol models are capable of treating only the two extreme mixing states of the generally mixed particle population. These are internal mixtures, wherein it is assumed that all particles having the same total mass have the same composition, and external mixtures, where, in the aerosol population, each particle arises from only one source (31). Most sectional models of the atmospheric aerosol are univariate in that they classify the particle population using only a single particle volume or mass coordinate. This representation generally forces the internal mixture approximation whereby $f(m_1, m_2, \ldots) \cong f(m)$, where m is the total particle mass. Thus it is assumed that all particles having the same total mass have the same composition (31). The bivariate methods presented here immediately provide a representation for a generally mixed aerosol population having two components and the fully bivariate distribution $f(m_1, m_2)$. The extension of moment methods, perhaps in combination with different methodologies such as MC, to higher order multivariate representations would have immediate and revolutionary implications for aerosol modeling.

We next consider an issue that is beyond the scope of the present paper yet important enough to mention. This concerns the accuracy with which moment methods, which track only the moments of the size distribution, can be used to predict suspended nanoparticle observables of physical interest. Indeed for univariate, spherical particles, the accuracy with which the physical/optical properties of the particle size distribution could be estimated using only the lower order tracked moments (generally to within a few percent) was cited in Section 1 above. For multivariate applications, we have seen in Sections 3 and 4 that the number of quadrature points required to achieve accurate representation of the dynamics is in general greater than that in the univariate case, and this in itself will tend to favor the accurate quadrature estimation of integrals of known kernel functions over a multivariate distribution using the lower order mixed moments. For example, assume that the property kernel can be approximated as a binomial summation, with arbitrary coefficients, over terms of the form $v^k a^l$, where both k and l can take on 1/3 integer values from 0 through 5/3. Under this approximation, it is easily seen that integration of this kernel over $n(u, v)$ reduces to summation over the 36 mixed moments tracked in Fig. 2 with the same coefficients (cf. Eq. [5]). For nonpolynomial kernels, such as optical kernels, kernels involving step functions (as might be used, for example, to evaluate the total mass of particles within a selected size range), and other complicated kernels over the size distribution, improved sampling methods such as the multiple isomomental distribution aerosol surrogate (MIDAS) technique (9) can be used. Indeed the combination of MIDAS with the univariate QMOM for dynamics has proven to be a very effective strategy for accurate estimation of physical and optical properties from the modeled moments of spherical particle distributions (9). Preliminary bivariate extension of the MIDAS method, based on a modification of the 12-point quadrature scheme present here, has already been achieved. This suggests that the bivariate mixed moments provide an efficient representation of the full bivariate distribution for properties estimation. The bivariate MIDAS will yield surrogates to the true bivariate distribution that exactly reproduce the known 36 bivariate moments. These surrogate distributions can then be integrated over the appropriate kernel functions, thereby providing what should be an effective modeling strategy for estimating the physical and optical properties of the (unknown) PSD from the modeled mixed moments. In future studies, the overall accuracy of physical and optical properties estimation will be evaluated for bivariate particle populations of complex morphology using a combination of the bivariate QMOM and MIDAS approaches.

The optimal design and control of nanoparticle synthesis reactors will require more realistic and computationally efficient simulation methods, both to facilitate efficient design/optimization/scale-up methods and to carry out practical

parameter estimation based on laboratory aerosol reactor data. Ideally, the methods developed to satisfy these immediate needs will carry over to turbulent flame synthesis reactors of industrial interest, and also apply equally well (with suitably modified rate laws) to nanoparticle synthesis either from the liquid phase or via supercritical fluids. What is clearly needed is a more efficient representation of complex multivariate particle populations, and one that lends itself to future incorporation into a computational fluid mechanics–based framework for reactor design. We believe that the quadrature-based MOM has the potential to accomplish this, and in this paper we have taken the first steps toward this end. Specifically, the extensions of the QMOM presented here have been shown to provide efficient and accurate modeling of the dynamics of bivariate particle populations. Only at much greater, if not prohibitive computational, expense can such results be obtained by explicit tracking of the bivariate distribution function, for example, by fully two-dimensional sectional methods. Moreover, our time-dependent results (illustrated in Figs. 1–3) would not be obtainable using purely "stochastic" techniques, such as Monte Carlo, which currently can only be used to obtain asymptotic results. On the other hand, we have demonstrated that, even in the bivariate case, it is possible to use the QMOM to rapidly model the approach to asymptotic behavior, allowing an immediate assessment of when the wealth of previously established asymptotic results can be applied to dynamical situations of interest—that is, when the assumption of "quasi–self-preservation" might be valid.

In this paper the nanoparticle size distribution has been represented by a subset of preselected lower order mixed moments whose evolution properties are readily determined using the bivariate QMOM. This approach has the attractive property that the evolution equations for these mixed moments can be embedded in a full PDF scheme for predicting particle dynamics in turbulent chemically reacting flows (32). Until now, computation fluid dynamic models based on PDF methods have been applied mainly to single-phase combustion systems, and extensions into the coupled particulate domain have been blocked by the formidable complexity of introducing an efficient "population balance solver." The above-mentioned multivariate extensions of the QMOM have the potential to circumvent this problem. In effect, the mixed moments would become additional state variables in, for example, a single-point PDF method for computing reactor performance. In our view this suggestion provides a rather promising path to the above-mentioned long-range goals of optimal reactor design and control.

ACKNOWLEDGMENTS

Research at BNL was supported in part by NASA through Interagency Agreement W-18,429 as part of its interdisciplinary research program on tropospheric aerosols and at Yale University through National Science Foundation Grant CTS-987 1885.

REFERENCES

1. Hulburt, H. M., and Katz, S., *Chem. Eng. Sci.* **19,** 555 (1964).
2. Friedlander, S. K., *Ann. New York Acad. Sci.* **404,** 354 (1983).
3. McGraw, R., and Saunders, J. H., *Aerosol Sci. Technol.* **3,** 367 (1984).
4. Frenklach, M., and Harris, S. J., *J. Colloid Interface Sci.* **118,** 252 (1987).
5. McGraw, R., *Aerosol Sci. Technol.* **27,** 255 (1997).
6. Barrett, J. C., and Webb, N. A., *J. Aerosol Sci.* **29,** 31 (1998).
7. McGraw, R., Huang, P. I., and Schwartz, S. E., *Geophys. Res. Lett.* **22,** 2929 (1995).
8. Yue, G. K., Lu, J., Mohnen, V. A., Wang, P.-H., Saxena, V. K., and Anderson, J., *Geophys. Res. Lett.* **24,** 651 (1997).
9. Wright, D. L., *J. Aerosol Sci.* **31,** 1 (2000).
10. Wright, D. L., McGraw, R., Benkovitz, C. M., and Schwartz, S. E., *Geophys. Res. Lett.* **27,** 967 (2000).
11. Tambour, Y., and Seinfeld, J., *J. Colloid Interface Sci.* **74,** 260 (1980). See also *J. Colloid Interface Sci.* **76,** 541.
12. Yu, S., and Kennedy, I. M., *Aerosol Sci. Technol.* **27,** 185 (1998).
13. McEnally, C. S., Schaffer, A. M., Long, M. B., Pfefferle, L. D., Smooke, M. D., Colket, M. B., and Hall, R. J., Twenty-Seventh Symposium (International) on Combustion, Combustion Inst., PA, p. 1497 (1998).
14. Xiong, Y., and Pratsinis, S. E., *J. Aerosol Sci.* **24,** 283 (1993).
15. Tsantilis, S., and Pratsinis, S. E., *AIChE J.* **46,** 407 (2000).
16. Xing, Y., Koylu, U. O., Tandon, P., and Rosner, D. E., *in* "Proc. Fifth World Congress of Chemical Engineering," Vol. V., p. 43. AIChE, San Diego, CA, July, 1996.
17. Xing, Y., Rosner, D. E., Koylu, U. O., and Tandon, P., *AIChE J.* **43,** 2641 (1997).
18. Xing, Y., Koylu, U. O., and Rosner, D. E., *J. Appl. Opt.* **38,** 2686 (1999).
19. Koch, W., and Friedlander, S. K., *J. Colloid Interface Sci.* **140,** 419 (1990).
20. Tandon, P., and Rosner, D. E., *J. Colloid Interface Sci.* **213,** 273 (1999).
21. Rosner, D. E., and Yu, S., *AIChE J.*, in press.
22. McGraw, R., and Wright, D. L., submitted for publication.
23. Seto, T., Hirota, A., Fujimoto, T., Shimada, M., and Okuyama, K., *Aerosol Sci. Technol.* **27,** 422 (1997).
24. Rosner, D. E., Tandon, P., McGraw, R., and Wright, D. L., *presented at* AIChE 2000 Particle Technology Forum, Los Angeles, CA, November, 2000, Paper T1d08, ISBN 0–8169–9896–5.
25. Pyykonen, J. private communication, 2000. (See also, Rosner, D. E., and Pyykonen, submitted for publication.)
26. Press, W. H., Vetterling, W. T., Teukolsky, S. A., and Flannery, B. P., "Numerical Recipes in FORTRAN" (Cambridge, Univ. Press New York, 1992.
27. Feller, W., An Introduction to Probability Theory and Its Applications, Vol. II, p. 155. Wiley, New York, 1971.
28. Simons, S., *J. Aerosol Sci.* **28,** 1393 (1997).
29. Vemury, S., Kusters, K. A., and Pratsinis, S. E., *J. Colloid Interface Sci.* **165,** 53 (1994).
30. Vemury, S., and Pratsinis, S. E., *J. Aerosol Sci.* **26,** 175 (1995). (See also, Filippov, A. V., Zurita, M., and Rosner, D. E., *J. Colloid. Interface Sci.* **229,** 261 (2000).
31. Seinfeld, J. H., and Pandis, S. N., "Atmospheric Chemistry and Physics: From Air Pollution to Climate Change," p. 1166. Wiley, New York, 1998.
32. Pope, S. B., *Prog. Energy Comb. Sci.* **11,** 119 (1985).